Chitosan Nanoparticle–Loaded Mannitol Microspheres: Structure and Surface Characterization

ARTICLE *in* BIOMACROMOLECULES · AUGUST 2007

Impact Factor: 5.75 · DOI: 10.1021/bm061131g · Source: PubMed

4 AUTHORS:

Ana Grenha
Universidade do Algarve
35 PUBLICATIONS **891** CITATIONS
SEE PROFILE

Begoña Seijo
University of Santiago de Compostela
55 PUBLICATIONS **1,848** CITATIONS
SEE PROFILE

C. Serra-Rodríguez
University of Vigo
66 PUBLICATIONS **934** CITATIONS
SEE PROFILE

Carmen Remuñán-López
University of Santiago de Compostela
47 PUBLICATIONS **2,943** CITATIONS
SEE PROFILE

Chitosan Nanoparticle-Loaded Mannitol Microspheres: Structure and Surface Characterization

Ana Grenha,[†] Begoña Seijo,[†] Carmen Serra,[‡] and Carmen Remuñán-López*,[†]

Department of Pharmacy and Pharmaceutical Technology, University of Santiago de Compostela, Faculty of Pharmacy, Campus Sur, 15782 Santiago de Compostela, Spain, and Center for Scientific and Technological Support to Research, University of Vigo, E-36310, Vigo, Spain

Received November 29, 2006; Revised Manuscript Received April 10, 2007

In this work, we aimed to characterize the surface and the internal structure of mannitol microspheres containing chitosan/tripolyphosphate nanoparticles, which were prepared by spray-drying. These microspheres were recently proposed as valuable candidates to transport therapeutic protein-loaded nanoparticles to the lungs owing to their favorable aerodynamic properties. To observe the distribution of chitosan nanoparticles and mannitol in the microspheres, specific characterization techniques, such as confocal laser scanning microscopy, X-ray photoelectron spectroscopy, and time-of-flight secondary ion mass spectrometry, were used. Results showed that mannitol is distributed in the whole particle and nanoparticles are homogeneously mixed with mannitol. Moreover, both components were detected in the microsphere surface, mannitol being present to a higher extent, which is in agreement with the theoretical mannitol/nanoparticle ratio of microspheres (80/20). Therefore, this work confirmed that chitosan nanoparticles were successfully encapsulated in mannitol microspheres, providing a homogeneous distribution of the nanoparticles and, hence, of the nanoencapsulated therapeutic macromolecule.

Introduction

Pulmonary systemic administration of therapeutic macromolecules is receiving increased attention due to several advantages such as the large lung surface available for absorption, the high blood flux and thin alveolar−vascular epithelium, the low proteolytic activity compared to other mucosal routes, and the possibility to avoid the first-pass effect.[1−3] In fact, several therapeutic macromolecules such as insulin,[4] parathyroid hormone,[5] and leuprolide,[6] have been described to be adequately absorbed through the lung epithelium. The requisite for a reliable and specific delivery to the lung is the use of powder carrier systems exhibiting adequate aerodynamic properties to reach the desired area. In this sense, microspheres have been extensively investigated, since they can be tailored to appropriate morphological and aerodynamic properties.[7] Nanoparticles have also been proposed as delivery systems for proteins and peptides to the lung epithelium[8−12] due to their ability to delay or avoid mucociliary clearance and macrophagic capture.[13,14] However, they present some limitations for this purpose, considering their reduced dimensions and mass, which make lung deposition a difficult issue, potentially exposing them to exhalation.[2,15−17] Furthermore, stability concerns due to the nanoparticle formulation as aqueous suspensions should also be taken into account. Our group has developed a new ionotropic gelation nanotechnology that is extremely mild and rapid and allows the production of chitosan-based nanoparticles.[18] These nanoparticles have been shown to possess an excellent capacity for protein entrapment and for improvement of mucosal peptide absorption through several epithelia such as the nasal[19] and intestinal.[20,21] Taking into account the above-mentioned limitations presented by the colloidal carriers for pulmonary administration, we proposed in a previous work the microencapsulation of protein-loaded chitosan nanoparticles using the carbohydrate mannitol as an attempt to improve their aerosolization to the lungs and to ensure their intact delivery at the drug absorption site, so that these restrictions could be solved.[12]

The obtained microspheres presented adequate aerodynamic properties for pulmonary delivery,[12] and it was recently demonstrated that they are biocompatible with two human cell lines representative of the respiratory bronchial (Calu-3) and alveolar (A549) epithelia, respectively.[22] Furthermore, the physicochemical properties of the microencapsulated nanoparticles and the release profile of insulin were shown to not be negatively affected by the spray-drying process, and nanoparticles could be easily recovered upon incubation of the microspheres in an aqueous medium.[12] However, in that work we did not address the question of the microsphere structure and, more specifically, the nanoparticle distribution within the microspheres.

It is of great interest to analyze and visualize the spatial distribution of the involved structures to confirm whether or not nanoparticles are homogeneously encapsulated in the microspheres and, hence, whether or not the nanoentrapped therapeutic protein is homogeneously distributed within the aerosolized powder. This will obviously influence the aerosol powder reproducibility and efficacy. In this manner, techniques such as confocal laser scanning microscopy (CLSM), X-ray photoelectron spectroscopy (XPS), and static time-of-flight secondary ion mass spectrometry (TOF-SIMS) should, altogether, provide information on the accurate characterization of the microspheres' internal and external structure. The main advantage of CLSM is the ability to provide visualization of images parallel to the sample surface at both internal and external levels, at multiple depths, without any mechanical sectioning. Nevertheless, the technique itself is not very precise in providing information on the most superficial composition of the microspheres. The surface region of a biomaterial, a

* Author to whom correspondence should be addressed. Phone: 0034 981 563100 Ext. 15405. Fax: 0034 981 547148. E-mail: ffcarelo@usc.es.
[†] University of Santiago de Compostela.
[‡] University of Vigo.

10.1021/bm061131g CCC: $37.00
Published on Web 06/22/2007

region only a few atomic layers deep, is the interface between the biomaterial and the biological environment, which triggers the sequence of biological events occurring when a biomaterial or biomedical device enters the organism. Furthermore, the determination of the microspheres' surface properties could be of great importance, given the knowledge that the chemical composition of a particle's surface governs interparticulate forces that influence dispersion of powder aerosols during inhalation.[23] Therefore, for a better understanding of the relation between surface properties and biological performance, it is necessary to characterize the biomaterial surface in detail. This entails determining the composition, structure, and distribution of all components present on the surface. Accurate surface characterization can be achieved using XPS and TOF-SIMS, which provide information on the chemical composition.

As mentioned previously, in a previous work we proposed mannitol microspheres as carriers of chitosan nanoparticles to the lung, the microspheres enabling an immediate release of the nanoparticles due to the high solubility of mannitol, which therefore only acts as an inert carrier of the nanoparticles. The aim of this work was to investigate the distribution of chitosan nanoparticles in mannitol microspheres and, hence, the nano-microparticulate system architecture. For this purpose, the inner structure of the microspheres was characterized using CLSM. Moreover, surface-sensitive analyses of the microspheres were performed using XPS and static TOF-SIMS to accurately characterize the microspheres' surface composition, determining whether nanoparticles are present.

Experimental Section

Materials. Chitosan (CS) in the form of hydrochloride salt (Protasan 213 Cl; deacetylation degree, 86%; viscosity, 95 mPa) was purchased from Pronova Biopolymer, A.S. (Norway). Pentasodium tripolyphosphate (TPP), glycerol, D-mannitol, phosphate-buffered saline (PBS) tablets, pH 7.4, and fluorescein isothiocyanate bovine serum albumin (FITC−BSA) were supplied by Sigma Chemicals (USA). Bodipy 630/650-X was obtained from Molecular Probes (Netherlands). Ultrapure water (Milli-Q Plus, Millipore Iberica, Spain) was used throughout.

Preparation of Chitosan Nanoparticles. CS/TPP nanoparticles were prepared according to the procedure developed by our group, based on the ionotropic gelation of CS with TPP anions, in which the positively charged amino groups of CS interact with the negatively charged TPP.[24] Briefly, CS and TPP were dissolved in purified water to obtain solutions of 1 mg/mL (w/v) and 0.69 mg/mL (w/v), respectively, to reach a final CS/TPP ratio of 3.6:1 (w/w). The spontaneous formation of nanoparticles occurs upon incorporation of 12 mL of the TPP solution into 30 mL of the CS solution, under gentle magnetic stirring at room temperature.

The FITC−BSA-loaded CS/TPP nanoparticles were obtained following the protein dissolution in purified water (0.9 mg FITC−BSA/0.6 mL H_2O) and incorporation in the TPP solution (pH 9.2) prior to the nanoparticles' formation. The protein concentration in the TPP solution was calculated to obtain nanoparticles with a theoretical content of 30% (w/w) FITC−BSA with respect to CS.

Nanoparticles were concentrated by centrifugation at 16 000*g* on a 10 μL glycerol bed for 30 min at 15 °C (Beckman Avanti 30, Beckman, USA). The supernatants were discarded, and nanoparticles were resuspended in 100 μL of purified water.

The nanoparticles' production yield was calculated by gravimetry. Fixed volumes of nanoparticle suspensions were centrifuged (16 000*g*, 30 min, 15 °C), and sediments were freeze-dried over 24 h at −34 °C, followed by a gradual increase in temperature until 20 °C, using a Labconco freeze dryer (Labconco, USA) ($n = 3$).

The process yield was calculated as follows

$$\text{process yield (\%)} = \frac{\text{nanoparticle weight}}{\text{total solids (CS + TPP + FITC−BSA) weight}} \times 100$$

Physicochemical Characterization of Nanoparticles. The morphological examination of CS/TPP nanoparticles was conducted by transmission electron microscopy (TEM) (CM 12 Philips, Eindhoven, Netherlands). The samples were stained with 2% (w/v) phosphotungstic acid and placed on copper grids with Formvar films for TEM observation.

Measurements of nanoparticles' size and zeta potential were performed on freshly prepared samples by photon correlation spectroscopy and laser doppler anemometry, respectively, using a Zetasizer 3000 HS (Malvern Instruments, Malvern, U. K.). For the particle size analysis, each sample was diluted to the appropriate concentration with filtered (0.2 μm filters Millex-GN, Millipore Iberica, Spain) ultrapure water. Each analysis lasted 180 s and was performed at 25 °C with a detection angle of 90°. For the determination of the electrophoretic mobility, samples were diluted with 0.1 mM KCl and placed in the electrophoretic cell, where a potential of ±150 mV was established. Three batches of each formulation were analyzed in triplicate ($n = 3$).

Determination of FITC−BSA Loading Capacity. The nanoparticles' association efficiency was determined upon separation of nanoparticles from the aqueous preparation medium containing the nonassociated protein by centrifugation (16 000*g*, 30 min, 15 °C). The amount of free FITC−BSA was determined in the supernatant measuring directly the absorbance by spectrophotometry (Shimadzu UV−vis spectrophotometer UV-1603, Japan) at 494 nm. A calibration curve was made using the supernatant of unloaded nanoparticles. Each sample was assayed in triplicate ($n = 3$). The nanoparticles' protein loading capacity and association efficiency were calculated as follows

$$\text{loading capacity (\%)} = \frac{\text{total FITC−BSA weight} - \text{free FITC−BSA weight}}{\text{nanoparticles' weight}} \times 100$$

$$\text{association efficiency (\%)} = \frac{\text{total FITC−BSA weight} - \text{free FITC−BSA weight}}{\text{total FITC−BSA weight}} \times 100$$

Preparation of Dry Powders Containing Chitosan Nanoparticles. Dry powders containing unloaded or FITC−BSA-loaded CS/TPP nanoparticles were obtained by spray-drying a suspension of CS/TPP nanoparticles in mannitol, as previously reported.[12] The nanoparticle suspension in mannitol was obtained by resuspending the nanoparticle sediments obtained after centrifugation, with an aqueous solution of mannitol, to achieve a theoretical mannitol/nanoparticle ratio of 80/20 (w/w) and a final solids content of 2.1% (w/v). This carbohydrate/nanoparticle ratio was chosen as it leads to the production of microparticles with adequate morphologic and aerodynamic characteristics for pulmonary administration.[12] When necessary, mannitol was previously stained with a fluorescent label to allow its visualization with confocal microscopy. The fluorophore Bodipy was added to the mannitol solution (167 μL of a 1 mg/mL solution of Bodipy; 0.32 μg Bodipy/mg mannitol) before nanoparticle resuspension, prior to spray-drying. The spray-drying process was performed using a laboratory-scale spray-dryer (Büchi mini spray dryer, B-290, Switzerland), under the following conditions: two fluids external mixing, 0.7 mm nozzle, feed rate of 2.5 mL/min, inlet and outlet temperatures of 160 ± 2 and 108 ± 3 °C, respectively. The air flow rate and the aspirator were kept constant at 400 NL/h and 80%, respectively. Dry powders were collected and stored in a desiccator at room temperature until use.

The spray-drying process yield was calculated by gravimetry, comparing the total solids weight with the resultant weight of microspheres after spray-drying, as follows ($n = 3$)

$$\text{process yield (\%)} = \frac{\text{microspheres weight}}{\text{total solids (CS + TPP + mannitol) weight}} \times 100$$

Microsphere Surface and Aerodynamic Characterization. *Morphological Analysis of Microspheres.* Microspheres were viewed using a scanning electron microscope (SEM, Leo 435VP, U. K.). Dry powders were placed onto metal plates and a 200-nm-thick gold palladium film was sputter-coated on the samples (high-resolution sputter coater SC7640, Termo VG Scientific, U. K.) before viewing. Furthermore, the Feret's diameter (distance between two tangents on opposite sides of the particle) was directly determined with an optical microscope (Olympus BH-2, Japan), this being estimated as the mean of 300 particles ($n = 300$).

Determination of Microsphere Density. Real density was determined using a helium pycnometer (micropycnometer, Quanta Chrome, model MPY-2, USA) ($n = 3$). The apparent tap density was obtained by measuring the volume of a known weight of powder in a 10 mL test tube after mechanical tapping (30 taps/min, Tecnociencia, Spain). After registration of the initial volume, the test tube was submitted to tapping until a constant volume was achieved, according to a previously described method[25] ($n = 3$).

Evaluation of Aerodynamic Diameter. Aerodynamic diameters were obtained using a TSI Aerosizer LD equipped with an Aerodisperser (Amherst Process Instruments, Inc., Amherst, MA, USA), which assumes that the particles have a spherical shape. Apparent density was used in this work. The equipment measuring principle is based on the measurement of the particles' time-of-flight ($n = 3$), according to the following equation

$$C_d \frac{\pi d^2}{4} \rho_a \frac{(V_a - V_p)}{2} = 1/6\, \pi d^3 \rho_p \frac{dV_p}{dt}$$

where C_d is the drag coefficient, d is the particle diameter, ρ_a is the density of air, V_a is the velocity of air, V_p is the velocity of particles, and ρ_p is the density of particles.

In Vitro Release Studies of FITC−BSA from Nanoparticles and Dry Powders. The release of FITC−BSA was determined by incubating the nanoparticles (CS/TPP 3.6:1) and the nanoparticle-loaded microspheres (mannitol/nanoparticles = 80/20, nanoparticles CS/TPP = 3.6:1) in 5 mL of pH 7.4 phosphate buffer (0.15 mg nanoparticles/mL, 0.75 mg microspheres/mL), with a horizontal mechanical shaker (Heidolph Promax 1020, Germany), at 37 °C. These studies were performed under sink conditions.

At appropriate time intervals (1, 2, 4, 6, and 8 days), individual samples were filtered (0.22 μm filters Millex-GV, low protein binding, Millipore Iberica, Spain), and the amount of protein released was evaluated in the supernatants by directly measuring the absorbance by spectrophotometry (Shimadzu UV−vis spectrophotometer UV-1603, Japan) at 494 nm ($n = 3$).

Structural Characterization of Nanoparticle-Loaded Microspheres Using CLSM. The internal structure of the nanoparticle-loaded microspheres was observed by CLSM, using a TCS-SP2 vertical microscope (Leica GmbH, Germany), which collects images using different detectors for fluorescent signals, which in this case were obtained by two laser lines: argon at 488 nm and helium−neon at 633 nm.

Small aliquots of the dry powder comprised of nanoparticle-loaded microspheres (nanoparticles loaded with FITC−BSA, mannitol-labeled with Bodipy) were placed on a glass slide, and a drop of immersion oil was added to avoid particle displacement during viewing. Laser excitation wavelengths of 488 and 633 nm were used to scan the powder, and fluorescent emissions from FITC−BSA (emission λ = 500−570 nm) and Bodipy (emission λ = 650−660 nm) were collected using separate channels. Images were acquired with a magnification of 100×, using an oil immersion lens (HCX PL Fluotar). The gray scale images obtained from each scan were pseudo-colored green (FITC-BSA) and red (Bodipy) and overlapped afterward (LCS Lite, Leica Confocal Software, Leica GmbH, Germany) to obtain a multicolored image.

Microsphere Surface Analysis Using XPS and TOF-SIMS. Blank (without encapsulated protein) nanoparticle-loaded mannitol microspheres and microspheres comprised only of mannitol were gently compacted into small stainless-steel troughs, and unloaded CS/TPP nanoparticles were placed directly on a polished monocrystalline silicon wafer used as a sample holder. The surface of these three samples was afterward analyzed using XPS (VG Escalab 250 iXL ESCA, VG Scientific, U. K.) and TOF-SIMS (TOF-SIMS IV, Ion-TOF GmbH, Germany). Mannitol microspheres and CS/TPP nanoparticles were used separately as controls. The XPS measurements were carried out using monochromatic Al−Kα radiation ($h\nu$ = 1486.92 eV), and photoelectrons were collected from a take-off angle of 90° relative to the sample surface. Measurements were performed in a constant analyzer energy (CAE) mode with a 100 eV pass energy for survey spectra and 20 eV pass energy for high-resolution spectra. Charge referencing was done by setting the lower binding energy C 1s photopeak at 285.0 eV C 1s hydrocarbon peak. The high-resolution spectra fitting is based on "χ-squared" algoritm used to determine the soundness of a peak fit. The experimental conditions (X-ray source, power, and analysis area) were kept constant for each analysis.

For TOF-SIMS analyses, samples were bombarded with a pulsed gallium primary ion beam (69 Ga^+) generated with a liquid metal ion gun operated at 15 kV and a 45° incidence with respect to the sample surface. The secondary ions generated were extracted with a 10 kV voltage, and their time-of-flight from the sample to the detector was measured in a reflectron mass spectrometer. Electron flood gun charge compensation was necessary during measurements. A raster size of 500 μm × 500 μm was used, and at least three different spots were analyzed under the "static" condition with ion doses of $\sim 10^{12}$ ions/cm^2. The calibration of the mass spectra in the positive mode was based on hydrocarbon peaks such as CH_2^+, CH_3^+, $C_2H_2^+$, and $C_3H_5^+$. The experimental conditions (ion type, beam voltage, and primary ion dose) were maintained constant for each experiment.

Statistical Analysis. The *t*-test was used to perform the statistical analysis. All analysis were run using the SigmaStat statistical program (version 3, Systat Software, USA), and differences were considered to be significant at a level of $p < 0.05$.

Results and Discussion

As stated in the Introduction, in this work we have performed a detailed characterization of a previously developed drug delivery system intended for pulmonary delivery, which consists in CS/TPP nanoparticles encapsulated in mannitol microspheres by a spray-drying technique. Extremely sensitive and accurate techniques of surface analysis such as XPS and TOF-SIMS were used to determine the microspheres' surface composition. Moreover, confocal microscopy was applied to evaluate the nanoparticles' distribution in the system; thus demonstrating the ability of the spray-drying technique to provide an adequate entrapment of the CS/TPP nanoparticles in inert carrier microspheres.

Preparation and Characterization of the Systems. CS/TPP nanoparticles were produced using CS and TPP solutions, by a very mild ionic gelation method, as described in the Experimental Section. Figure 1 displays the TEM microphotograph of representative CS/TPP nanoparticles, showing that these are spherical and compact.

Table 1 depicts the physicochemical characteristics of unloaded (without encapsulated protein) and FITC−BSA-loaded CS/TPP nanoparticles, FITC−BSA being selected as a model and labeling protein. The nanoparticles, produced with a process yield of 55−60%, present a size between 300 and 380 nm and

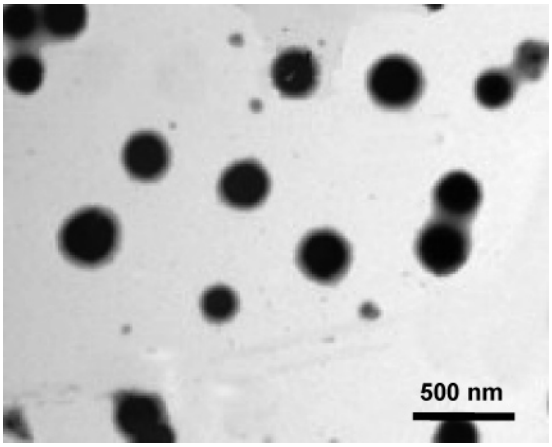

Figure 1. TEM micrograph of unloaded chitosan nanoparticles.

Table 1. Process Yields and Physicochemical Properties of Unloaded (without Protein) and FITC−BSA-Loaded Nanoparticles (Mean ± Standard Deviation, $n = 3$)

formulation	process yield[a] (%)	size (nm)	zeta potential (mV)	association efficiency[b] (%)	loading capacity[c] (%)
unloaded	60 ± 4	300 ± 17	+34.3 ± 1.5		
FITC−BSA-loaded	55 ± 8	382 ± 16	+33.5 ± 3.3	89 ± 4	31 ± 1

[a] Process yield (%) = [nanoparticle weight/total solids weight] × 100. [b] Association efficiency (%) = [(total FITC−BSA amount − free FITC−BSA)/total FITC−BSA amount] × 100. [c] Loading capacity (%) = [(total FITC−BSA amount − free FITC−BSA)/nanoparticle weight] × 100.

a positive zeta potential of approximately +34 mV. As expected, FITC−BSA was successfully encapsulated in CS/TPP nanoparticles with an association efficiency of approximately 90% and a loading capacity as high as 31%. Protein incorporation did not lead to changes in the production yield or zeta potential. However, nanoparticle size showed a slight, although significant ($p < 0.05$), increase with the protein incorporation which, however, did not compromise our objectives.

The aerodynamic behavior of a powder intended for pulmonary administration is the key factor for the particles to be successfully inhaled, although morphological characteristics, which may interfere in the powder aggregation and flowing properties, also play an important role. CS/TPP nanoparticle-loaded mannitol microspheres were previously described as an outstanding drug delivery system of proteins by the pulmonary route, given the adequate morphological and aerodynamic properties presented by these powders and their ability to release nanoparticles, and consequently the encapsulated peptide insulin, upon contact with an aqueous medium.[12] As can be observed in the SEM microphotograph depicted in Figure 2, microspheres obtained by spray-drying are spherical, not being aggregated, and they further present a smooth surface.

The aerodynamic diameter, which is a combination of the particle size, density, and shape, influences the dispersion and sedimentation patterns and should vary between 1 and 5 μm to allow an optimal lung deposition.[3,7] Microspheres produced in this work presented a Feret diameter of 3.1 ± 1.2 μm, real density of approximately 1.5 g/cm^3, and a tap density as low as 0.3 g/cm^3, which rendered a mean aerodynamic diameter of 2.71 ± 0.06 μm, adequate for lung delivery.

FITC−BSA was not released from the nanoparticles or nanoparticle-loaded microspheres throughout the 8 days. The lower or absent release of FITC from chitosan nanoparticles was also reported by Huang et al., who registered a maximum release of 1% in 24 h at pH 7.4.[26] The aqueous diffusion coefficient of a molecule is inversely related to its molecular weight,[27] and it is likely that the high molecular weight of FITC−BSA (67 KDa) is responsible for the hindrance of its diffusion through the chitosan nanoparticles. Chitosan nanoparticles present a hydrogel structure, and the existent mesh space in the hydrogel, which enables molecular diffusion, is responsible for the size exclusion process for the associated molecules that release by this mechanism. The mesh can change from the collapsed to the swollen state, depending on the pH.[28] As the swelling of chitosan is greatly reduced at pH 7.4, selected to perform the in vitro release studies, it is possible that the mesh sizes available for the diffusion of FITC−BSA, which presents a size of 7.2 nm, were too small, thus preventing the release of the protein. Therefore, taking into account this absence of release, the satisfactory selection of FITC−BSA as a labeling protein to perform the subsequent studies of nanoparticle-loaded microspheres structural characterization by confocal microscopy was confirmed.

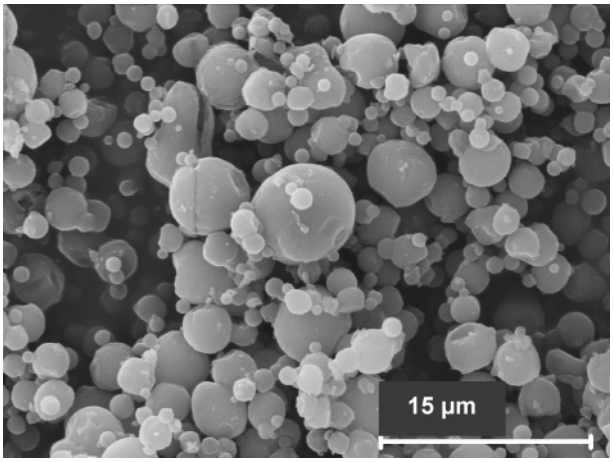

Figure 2. SEM micrograph of microspheres prepared with a mannitol/nanoparticle (Ma/NP) theoretical ratio of 80/20 and a solids content of 2.1%.

Structural Characterization of Nanoparticle-Loaded Microspheres. From the observation of the SEM micrograph shown in Figure 2, we could see that the produced dry powders have a spherical shape, as mentioned above. However, the SEM technique was not able to provide evidence on the nanoparticles' localization in the microspheres. In contrast, the application of a technique such as confocal microscopy permitted more clear information on the microspheres' structure, and using different fluorescent labels for each independent structure to be analyzed, marked compounds could be identified unambiguously. Concerning the characterization of drug delivery systems, this technique has already been applied to determine the localization of nanoparticles incorporated in microspheres.[11,29] Figure 3A shows three micrographs corresponding to a cross-section of a microsphere, where from left to right are shown the red channel (A1), which detects the signal of mannitol labeled with Bodipy, the green channel (A2), which detects the signal emitted by the FITC−BSA-labeled nanoparticles and, finally, the overlapping of both channels (A3). Figure 3B depicts three different sections in a series, obtained by varying values in the *z*-axis, each section being separated from the subsequent one by 0.8 μm. From B1 to B3, the detector is moving from the middle of the microsphere to one of the tops. From the observation of these images (Figures 3A and 3B), we could deduce that mannitol is distributed within the whole particle, forming a kind of continuous matrix, where the nanoparticles are homogeneously dispersed.

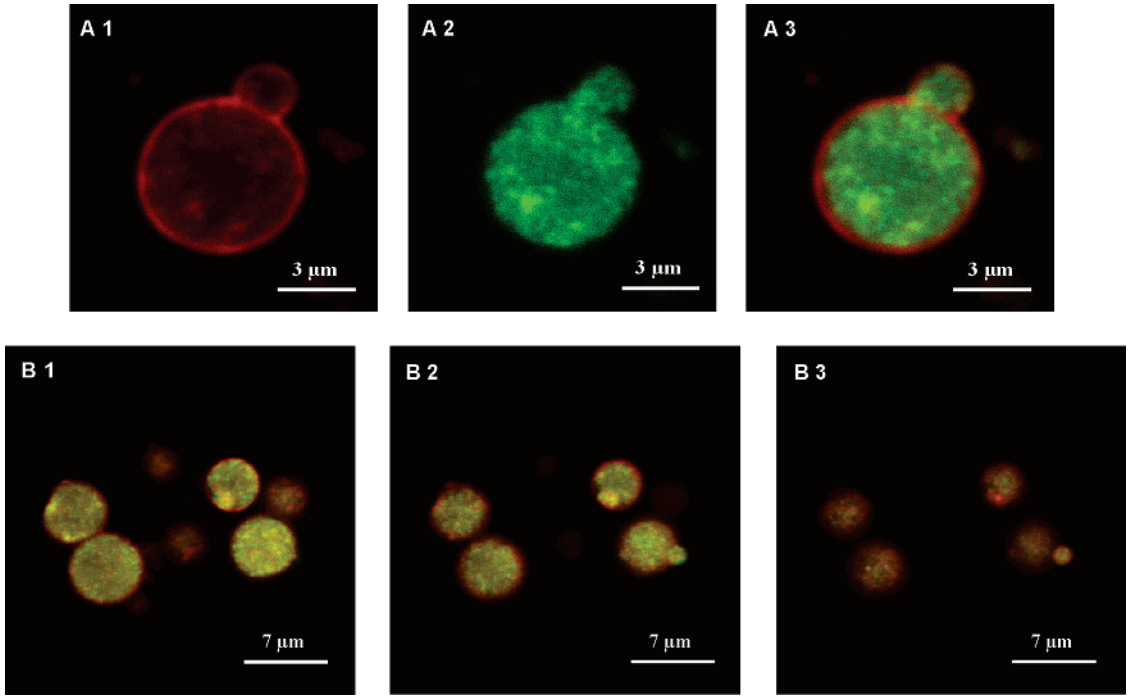

Figure 3. Confocal imaging of microspheres, prepared with mannitol stained with Bodipy (red) and nanoparticles labeled with FITC−BSA (green): A1, red channel; A2, green channel; A3, overlapping of both channels. B1, B2, and B3 correspond to the overlapping of both channels in different sections of the same series, separated in the *z*-axis by 0.8 μm.

Similar results were obtained by Sham et al., when preparing dry powders comprised of lactose and polycyanoacrylate nanoparticles. In their study, the nanoparticles were distributed within the whole microsphere, as occurs in our case, but the main difference is that our nanoparticles are evenly dispersed while theirs tended to accumulate in clusters, an effect that they explained as a result of the adhesive nature and the surface energy of the nanoparticles.[11] In the present work, CLSM images suggested that nanoparticles are efficiently encapsulated in the microsphere, being completely coated by a mannitol layer, which apparently forms a structure similar to a wall. Using this technique, the presence of nanoparticles in the outer side of the microspheres was not detected, since the most external signal detected is the red one, corresponding to mannitol. This wall effect was previously found by Cook et al. when encapsulating, using spray-drying, terbutaline nanoparticles in hydrophobic microspheres comprised of hydrogenated palm oil and dipalmitoylphosphatidylcholine. Also using CLSM as a technique, they determined the absence of nanoparticles in the first 400 nm of the microspheres as well as a complete external layer of the hydrophobic components.[29]

In this work, most of the observed particles demonstrated the presence of mannitol and CS/TPP nanoparticles within the whole particle, albeit during the confocal scanning of the powders a few hollow microspheres could be visualized (Figure 4). This observation corroborates the results presented in our previous paper, in which SEM micrographs of some broken and hollow microspheres were shown.[12] It is important to notice that this occurred punctually and mostly for particles much larger than the mean size, which generally demonstrated some kind of a hole or breach. In fact, the produced dry powder is mainly constituted of solid microspheres, which was also suggested by the high value obtained for the real density (1.57 g/cm^3), as proposed elsewhere.[30]

Microsphere Surface Analysis. As commented above, CLSM images suggested that mannitol completely involved the nanoparticles, being present as an external shell of the microspheres. Although high-resolution images could be obtained with this microscopy technique, it did not allow an accurate analysis of the surface composition of the microspheres, which would be a determinant to know the localization of nanoparticles and mannitol. As it has been previously commented, the determination of these surface properties could be of major importance from the point of view of the behavior of powder aerosols during

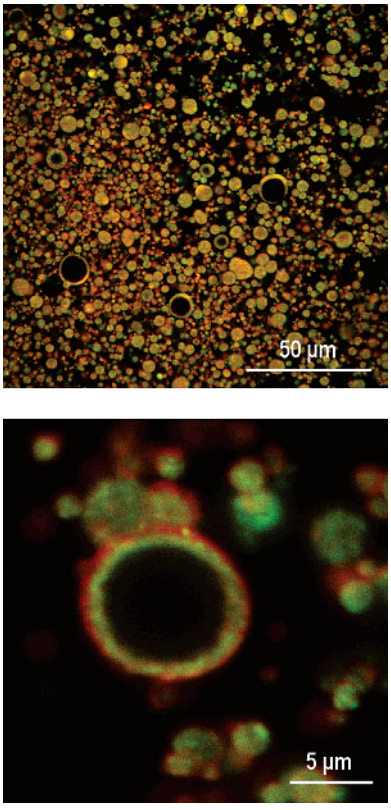

Figure 4. Confocal images of hollow microspheres, showing overlapping of green and red channels.

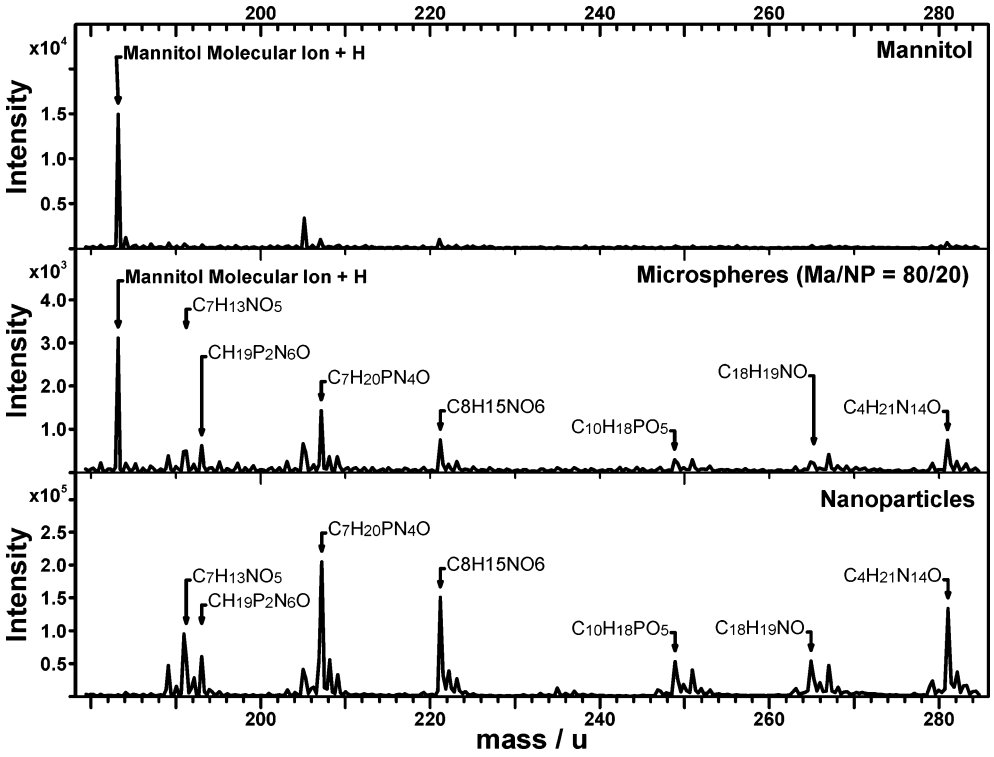

Figure 5. Mass spectra obtained by TOF-SIMS of control mannitol, nanoparticle-loaded microspheres (mannitol/nanoparticles (Ma/NP) = 80/20), and control CS/TPP nanoparticles.

Table 2. Surface Composition (Atomic Percentage), Determined by XPS, of CS/TPP Nanoparticles, Mannitol, and Microspheres (Mannitol/Nanoparticles = 80/20)

element	CS/TPP nanoparticles (%)	mannitol (%)	microspheres (%)
C	53.8	56.2	54.9
O	33.8	43.8	43.3
N	4.5	0	0.6
P	2.7	0	0
Si	5.2	0	1.2
ratio N/C	0.084	0	0.011
ratio C/O	1.592	1.283	1.268

inhalation as well as of their biological performance. In this manner, specific techniques of surface analysis, such as XPS or TOF-SIMS, which deal with the determination of the chemical elements present in the most superficial layer of the samples and in this case of the microspheres, should provide us with unquestionable information on the surface composition.

XPS is one of the most commonly used techniques of surface analysis. Upon exposition of the sample to an X-ray beam, the binding energies of characteristically emitted photoelectrons are measured, providing information on the elements from which they originate as well as their chemical bonding.[31] XPS has been extensively used in the field of biomedical research with different aims such as characterization of polyurethane membranes for cardiovascular application,[32] confirmation of chitosan and gelatin coating on polylactide-*co*-glycolide acid (PLGA) surfaces,[33] and determination of surface composition of microspheres and nanoparticles.[23,24,34]

Table 2 displays the results obtained by the XPS analysis of surfaces of control nanoparticles, control mannitol, and microspheres containing both nanoparticles and mannitol, the percentage of each chemical element present in the sample being determined. The survey of control CS/TPP nanoparticles detected the expected elements, such as C, N, P, and O, albeit traces of Si were also found, which could be a result of the Si-based sample holder substrate or a consequence of the processing of the exoskeleton components from the original material, as reported elsewhere.[35] The assay detected in the nanoparticles approximately 54% C and 34% O. Moreover, 5% N and 3% P were detected, which correspond to the presence of, respectively, CS and the cross-linking agent TPP. The obtained atomic percentages were comparable to those previously reported by Matienzo and Winnacker when analyzing chitosan films (61% C, 31% O, and 6% N), although slight differences could be explained by the use of chitosans with different deacetylation degrees (86% in our case vs 70% in theirs) as well as by the fact that we analyzed chitosan nanoparticles containing TPP, while they assayed pure chitosan films.[35] Furthermore, in our work, a C/O ratio of approximately 1.6 was obtained, which is similar to the 1.4 that was found by Calvo et al. in a study with CS nanoparticles (CS/TPP = 4.4:1). In addition, we found a C/N ratio of 11.9, which is slightly higher than that obtained by Calvo et al. (10.9) and which reflects the lower amount of chitosan that we used (CS/TPP = 3.6:1 vs 4.4:1 used in the referred study).[24]

As expected, the analysis of the control mannitol only detected signals of C (56%) and O (44%), typical elements of this substance, the C/O ratio being 1.283. When analyzing the surface of microspheres containing mannitol and CS/TPP nanoparticles, high amounts of C and O were detected, but also small amounts of N, an element exclusive to the nanoparticles, were found. However, it should be noted that the amount of N detected in the control nanoparticles was 4.5%, while in the microspheres only 0.6% was identified, indicating the presence of less nanoparticles in the latter. Moreover, a Si signal was also identified, which as previously said could be attributed to the processing of chitin shells and, therefore, to the presence of chitosan. Despite the fact that this indicates the presence of nanoparticles in the microsphere surface, it is important to notice

that the C/O ratio found in the microspheres is very similar to that of control mannitol (1.283 and 1.268, respectively). This indicates that the microsphere surface is mostly composed of mannitol, but nanoparticles are also detected, though to a lower extent, which is consistent with the mannitol/nanoparticle ratio (mannitol/nanoparticles = 80/20) composing microspheres.

In contrast to electron spectroscopy techniques such as XPS, TOF-SIMS not only provides information on the elements present but also offers detailed molecular information with high sensitivity. The sample surface is impinged by ions of some energy, which causes the emission of intact molecules that are specific to the uppermost monolayer of the surface, usually varying between 2 and 5 nm.[36,37] This technique is much more recent than XPS, so its application in drug delivery is less extended. Nevertheless, it has been used a few times to characterize surfaces of particles or powders, such as polystyrene or cellulose beads.[38,39]

Figure 5 displays the positive mass spectra between 180 and 290 amu, obtained by TOF-SIMS for each of the analyzed samples. The obtained results corroborated those previously observed by XPS, indicating that there is a high resemblance between the elemental composition of the control mannitol and microspheres containing mannitol and nanoparticles. In fact, we could observe masses (M) which have been reported as specific and typical of mannitol, such as the M183 (molecular ion + H^+) in both mannitol and microspheres containing nanoparticles.[40] However, comparing the spectra of microspheres with that of control nanoparticles, similar masses, which correspond to positive ions characteristic of the nanoparticles, can be identified in both samples. Given the absence of bibliographic support on the typical masses of this mixture CS/TPP, we assume that characteristic ions from nanoparticles are those identified in their spectra, which should appear in the microsphere spectrum in the case that nanoparticles are detected in the microsphere surface. These characteristic ions, such as M193 ($CH_{19}P_2N_6O$), M249 ($C_{10}H_{18}PO_5$), and M281 ($C_4H_{21}N_{14}O$), among others, result from the starting material (CS and TPP) and can arise from the fragmentation of both compounds, from the fragmentation of the phosphated polymer if there is any chemical reaction between CS and TPP, or even from the association of fragments of both. Moreover, M221.2 was further detected in the microspheres, possibly being due to the *N*-acetyl-D-glucosamine molecular ion ($C_8H_{15}NO_6$), which is the basic unit of chitosan molecules.[40]

Considering the intensities of the referred peaks and comparing them in the spectra of each sample, it was demonstrated that although much of the surface is covered by mannitol nanoparticles could also be detected. Given the novelty of this technique, no references were found reporting results of the application of TOF-SIMS on this material, and thus, the establishment of comparisons with previous developed works was not possible.

A global analysis of the results obtained by XPS and TOF-SIMS indicated that mannitol constitutes the most part of the microspheres surface and that nanoparticles were detected to a lower extent. Moreover, these results are in agreement with a homogeneous distribution of the nanoparticles in the microspheres, as suggested by the CLSM technique.

Conclusions

In this work, microspheres containing chitosan nanoparticles dispersed in mannitol were structurally characterized using innovative techniques such as CLSM, XPS, and TOF-SIMS. The examination by CLSM indicated that the nanoparticles were efficiently encapsulated in the microspheres, being homogeneously distributed within the whole particle. Moreover, the specific and accurate analysis of the microsphere surface using extremely surface-sensitive techniques such as XPS and TOF-SIMS demonstrated the presence of mannitol and nanoparticles on the microsphere surface, a higher proportion of mannitol being detected, in agreement with the theoretical mannitol/nanoparticle ratio of the microspheres. Therefore, it was confirmed that this drug delivery system is a promising carrier of protein-loaded nanoparticles and, hence, of therapeutic proteins to the lung.

Acknowledgment. This work was supported by the Spanish Government (CICYT, SAF2002-03314, Feder cofinanced) and Xunta de Galicia (PGIDIT Incentivo Plan Nacional del Proyecto SAF2002-03314). The predoctoral fellowship (SFRH/BD/13119/2003) to A.G. from the Fundação para a Ciência e Tecnologia, Portugal, is highly appreciated.

References and Notes

(1) Edwards, D. A.; Ben-Jebria, A.; Langer, R. *J. Appl. Physiol.* **1998**, *84*, 379−385.
(2) Clark, A. *Drug Delivery Syst. Sci.* **2002**, *2*, 73−77.
(3) Courrier, H. M.; Butz, N.; Vandamme, T. F. *Crit. Rev. Ther. Drug Carrier Syst.* **2002**, *19*, 425−498.
(4) Edwards, D. A.; Hanes, J.; Caponetti, G.; Hrkach, J.; Ben-Jebria, A.; Eskew, M. L.; Mintzes, J.; Deaver, D.; Lotan, N.; Langer, R. *Science* **1997**, *276*, 1868−1871.
(5) Codrons, V.; Vanderbist, F.; Ucakar, B.; Préat, V.; Vanbever, R. *J. Pharm. Sci.* **2004**, *93*, 1241−1252.
(6) Alcock, R.; Blair, J. A.; O'Mahony, D. J.; Raoof, A.; Quirk, A. V. *J. Controlled Release* **2002**, *82*, 429−440.
(7) Taylor, G.; Kellaway, I. In *Drug Delivery and Targeting: For Pharmacists and Pharmaceutical Scientists*; Hillery, A., Lloyd, A., Swarbrick, J., Eds.; Taylor & Francis: New York, 2001; p 269.
(8) Zhang, Q.; Shen, Z.; Nagai, T. *Int. J. Pharm.* **2001**, *218*, 75−80.
(9) Tsapis, N.; Bennet, D.; Jackson, B.; Weitz, D. A.; Edwards, D. A. *Proc. Natl. Acad. Sci. U.S.A.* **2002**, *99*, 12001−12005.
(10) Dailey, L. A.; Schmehl, T.; Gessler, T.; Wittmar, M.; Grimminger, F.; Seeger, W.; Kissel, T. *J. Controlled Release* **2003**, *86*, 131−144.
(11) Sham, J. O.; Zhang, Y.; Finlay, W. H.; Roa, W. H.; Löbenberg, R. *Int. J. Pharm.* **2004**, *269*, 457−467.
(12) Grenha, A.; Seijo, B.; Remuñan-Lopez, C. *Eur. J. Pharm. Sci.* **2005**, *25*, 427−437.
(13) Makino, K.; Yamamoto, N.; Higuchi, K.; Harada, N.; Ohshima, H.; Terada, H. *Colloids Surf., B* **2003**, *27*, 33−39.
(14) Schurch, S.; Gehr, P.; Im Hof, V.; Geiser, M.; Green, F. *Respir. Physiol.* **1990**, *80*, 17−32.
(15) Heyder, J.; Gebhart, J.; Rudolf, G.; Schiller, C. F.; Stahlhofen, W. *J. Aerosol Sci.* **1986**, *17*, 811−825.
(16) Finlay, W. H.; Stapleton, K. W.; Zuberbuhler, P. *J. Aerosol Sci.* **1997**, *28*, 1301−1309.
(17) Finlay, W. H.; Gehmlich, M. G. *Int. J. Pharm.* **2000**, *210*, 83−95.
(18) Calvo, P.; Remuñan-Lopez, C.; Vila-Jato, J. L.; Alonso, M. J. *Pharm. Res.* **1997**, *14*, 1431−1436.
(19) Fernandez-Urrusuno, R.; Calvo, P.; Remuñan-Lopez, C.; Vila-Jato, J. L.; Alonso, M. J. *Pharm. Res.* **1999**, *16*, 1576−1581.
(20) Alonso-Sande, M.; Cuña, M.; Remuñán-López, C.; Teijeiro-Osorio, D.; Alonso-Lebrero, J. L.; Alonso, M. J. *Macromolecules* **2006**, *39*, 4152−4158.
(21) Cuña, M.; Alonso-Sande, M.; Remuñan-Lopez, C.; Pivel, J. P.; Alonso-Lebrero, J. L.; Alonso, M. J. *J. Nanosci. Nanotechnol.* **2006**, *6*, 2887−2895.
(22) Grenha, A.; Grainger, C.I.; Dailey, L.A.; Seijo, B.; Martin, G.P.; Remuñán-López, C.; Forbes, B. *Eur. J. Pharm. Sci.* **2007**, *31*, 73−84.
(23) Bosquillon, C.; Rouxhet, P. G.; Ahimou, F.; Simon, D.; Culot, C.; Préat, V.; Vanbever, R. *J. Controlled Release* **2004**, *99*, 357−367.
(24) Calvo, P.; Remuñan-Lopez, C.; Vila-Jato, J. L.; Alonso, M. J. *J. Appl. Polym. Sci.* **1997**, *63*, 125−132.
(25) El-Gibaly, I. *Int. J. Pharm.* **2002**, *294*, 7−21.

(26) Huang, M.; Zengshuan, M.; Khor, E.; Lim, L.-Y. *Pharm. Res.* **2002**, *19*, 1488−1494.
(27) Polson, A. *J. Phys. Chem.* **1950**, *54*, 649−652.
(28) Peppas, N. A. *Curr. Opin. Colloid. Interface Sci.* **1997**, *2*, 531−537.
(29) Cook, R. O.; Pannu, R. K.; Kellaway, I. W. *J. Controlled Release* **2005**, *104*, 79−90.
(30) Gilani, K.; Najafabadi, A. R.; Barghi, M.; Rafiee-Tehrani, M. *Eur. J. Pharm. Biopharm.* **2004**, *58*, 595−606.
(31) Turner, N. H.; Schreifels, J. A. *Anal. Chem.* **1998**, *70*, 229R−250R.
(32) Lin, W.-C.; Tseng, C.-H.; Yang, M.-C. *Macromol. Biosci.* **2005**, *5*, 1013−1021.
(33) Zhu, A. P.; Fang, N.; Chan-Park, M. B.; Chan, V. *Biomaterials* **2006**, *27*, 2566−2576.
(34) Dong, Y.; Feng, S. *Biomaterials* **2004**, *25*, 2843−2849.
(35) Matienzo, L. J.; Winnacker, S. K. *Macromol. Mater. Eng.* **2002**, *287*, 871−880.
(36) Hagenhoff, B. *Mikrochim. Acta* **2000**, *132*, 259−271.
(37) Belu, A. M.; Graham, D. J.; Castner, D. G. *Biomaterials* **2003**, *24*, 3635−3653.
(38) Davies, M. C.; Brown, A.; Newton, J. M.; Chapman, S. R. *Surf. Interface Anal.* **1988**, *11*, 591−595.
(39) John, C. M.; Odom, R. W.; Salvati, L.; Annapragada, Ananth V.; Lu, M. Y. F. *Anal. Chem.* **1995**, *67*, 3871−3878.
(40) *NIST Chemistry WebBook, NIST Standard Reference Database*; Linstrom, P. J., Mallard, W. G., Eds.; National Institute of Standards and Technology: Gaithersburg, MD, 2005. http://webbook.nist.gov.

BM061131G